Analysis of LIGO/Virgo Gravitational Waves data

~~Internship report Master 2 March Jun 2020~~

~~Edited~~ By

Sylvian Lequeux

Institut des deux infinis , CNRS/IP2I, Université de Lyon, Université Claude Bernard Lyon 1, F-69622 Villeurbanne Cedex, France

Supervisor: Viola Soridini, IP2I Virgo group

Contents

Chapter 1

Introduction

This report documents my internship in the IP2I Virgo group, during which i have worked on data analysis for searches for Gravitational Waves (GW) signals from compact binaries coalescences (CBC).

1.1 Gravitational Waves

1.1.1 Historical introduction

Gravitational waves have been predicted theoretically by Einstein in his general theory of gravitation in 1916. They are waves solutions of the equations which physically represent a perturbation of the space time himself like a wave on the water. These objects are very hard for experiments to detect because of the smallness of their amplitude $\approx 10^{-20}$-10^{-25}.That's why,there was no evidence of their existence until 2015 but only indirect proofs such as the study of the pulsar PSR1913+16.

It's only in 2015,that the signal of a GW was for the first time detected by LIGO. This was a tremendous achievement for GW terrestrial interferometers and a milestone for the gravitational waves physics for which three eminent physicist of the LIGO/Virgo collaborations have received the Nobel Prize in Physics in 2017.

With LIGO and Virgo taking data and detecting more and more events, with particularly one example of multi-messenger analysis of a Binary Neutron Starts coalescence in 2017 [1], GW are a very active area of physics and a very promising one. Indeed, GW are a new messenger allowing us to explore the Universe in an unprecedented way with implications for nuclear physics, cosmology for instance, and plenty of room for new discoveries.

1.1.2 Theory of Gravitational Waves

To obtain a theoretical expression of a GW,we must start with the non linear equation of general relativity:

$$R_{\mu\nu} - \frac{1}{2} g_{\mu\nu} R = -\frac{8\pi G}{c^4} T_{\mu\nu} \tag{1.1}$$

where $R_{\mu\nu}$ is the Ricci curvature tensor, R the scalar curvature,$g_{\mu\nu}$ the metric tensor and $T_{\mu\nu}$ the stress-energy tensor.

In the weak filed approximation, the curvature can be written as Minkowski curvature which corresponds to a flat space. So, the metric tensor can be written as:

$$g_{\mu\nu} = \eta_{\mu\nu} + h_{\mu\nu} \tag{1.2}$$

where $\eta_{\mu\nu}$ is the Minkowski tensor (with $c = 1$):

$$\eta_{\mu\nu} = \begin{pmatrix} -1 & 0 & 0 & 0 \\ 0 & 1 & 0 & 0 \\ 0 & 0 & 1 & 0 \\ 0 & 0 & 0 & 1 \end{pmatrix} \tag{1.3}$$

and $h_{\mu\nu} \ll 1$ is the perturbation.

After few calculations and some adjustments in the equations , especially if we want GW in vacuum ($T_{\mu\nu} = 0$), we obtain:

$$\Box \bar{h}_{\mu\nu} = 0 \Leftrightarrow \{\nabla - \frac{\partial^2}{\partial t^2}\} \bar{h}_{\mu\nu} = 0 \tag{1.4}$$

with $\bar{h}_{\mu\nu} \equiv h_{\mu\nu} - \frac{1}{2}\eta_{\mu\nu} h_{\alpha\beta} \eta^{\alpha\beta}$.

We recognize a wave equation which by definition admits waves solutions:

$$\bar{h}_{\mu\nu} = Re\{A_{\mu\nu} e^{ik_\rho x^\rho}\} \tag{1.5}$$

with $A_{\mu\nu}$ the amplitude of the wave and k_ρ the wave factor.

This simplified calculation shows that GW are a natural consequences of Einstein's equations. In reality, the calculations are quite more complex because we aren't in vacuum so we have to conserve the tensor $T_{\mu\nu}$ and the effect of very strong gravitational field, for example in binary systems, has to be taken into account.

In real life, for compact Binary coalescences , post-Newtonian expansion are used to find approximate solutions to the Einstein's equations, and describe quite well the so-called inspiral phase as illustrated in Figure 1.1. When the gravitational field becomes too strong, the solutions needs numerical relativity calculations. The combination of these two ingredients can give predictions of GW waveforms, that

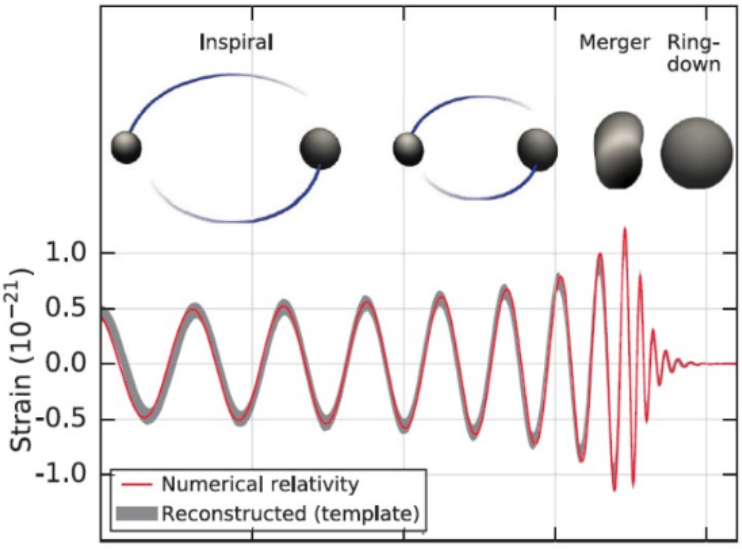

Figure 1.1: Example of Binary Black Hole template

are often called "templates". The shape of a given template depends on many parameters such as the type of objects involved in the coalescence, their mass and spins. For example, the larger the masses of the objects are, the shorter is the signal and its amplitude higher. Also, closer the source is, higher is the amplitude of the signal coming from the source but its shape doesn't change.

1.1.3 Sources of Gravitational Waves

It exists several objects that theoretically are expected to emit gravitational waves. The GW signal associated to them can be transient or continuous, but they all have in common that they can help us to learn a lot about our Universe or even more. Let's describe few of them:

-Supernovae: such as supernovae of type II which are the result of the collapsing of massive stars that creates a neutron star or a black hole. If this process isn't symmetric, GW will be emitted from the object but their detection are difficult because the determination of the shape of these GW emission is still hard to predict.

-Binary systems of compact objects (CBC): mainly composed by neutron stars and black holes, both objects turn around each other by emitting GW. The system is therefore losing energy, which decreases the distance between both objects and increases their rotation velocity until they enter the coalescence phase where they mix each other up to form only one object.

-Continuous waves sources: spinning neutron stars with asymmetry or surface irregularity would emit a periodic signal.

-Stochastic background: it is the equivalent of the cosmic microwave back-

ground but with the first emission of GW in the primordial universe. The detection of this signal could teach us a lot about the early beginning of the Universe.

-all others exotic sources including unknowns.

The LIGO/Virgo community is very active to search for all these signals. As of today, only signals from CBC have been detected. We will only deal with these particular systems in this report.

In conclusion, GW are a new messenger allowing us to explore the Universe and their study has important implications in many fields, as nuclear physics (helping to understand the equation of state of super-dense matter in Neutron Stars) , cosmology (measuring the Hubble parameter) or Gravity (test in strong fields of General relativity).

1.2 Detection with LIGO/Virgo

1.2.1 Principle of optical interferometry

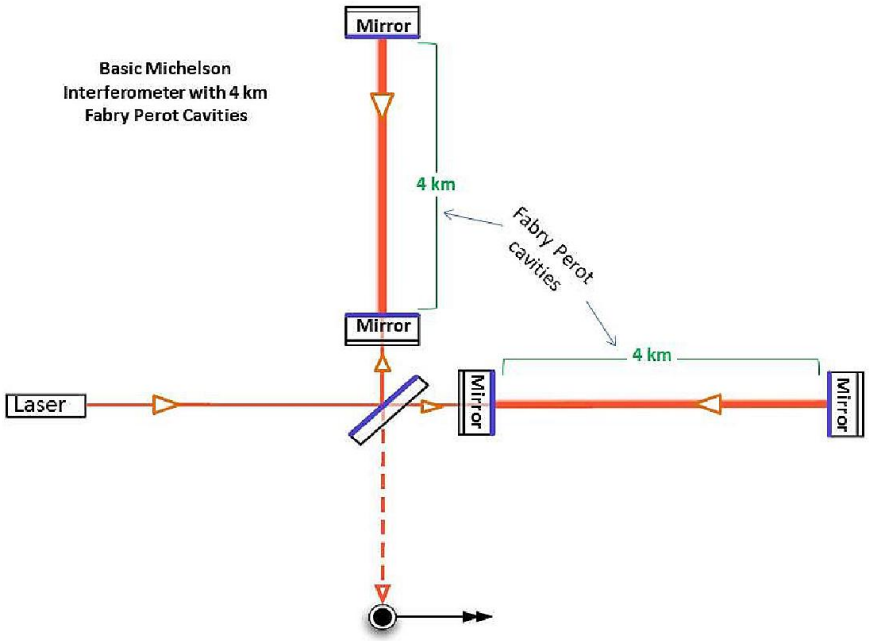

Figure 1.2: Schema of the Michelson Interferometer

LIGO and Virgo network consists of three interferometers: two LIGO in the USA (the LIGO Handford and Livingston Observatories, also noted LHO and LLO respectively) and one in Italy named Virgo. They work on the principle of a Michelson interferometer with two perpendicular arms, which are several kilometers long (4

for LIGO and 3 for Virgo). As we can see in Figure 1.2, both arms have a Fabry-Perot cavity which allows to extend the light travelled length in order to get a better sensitivity (Michelson sensitivity is inversely proportional to the travelled length of the light in the arms).

The passing of a GW is highlighted by detecting the induced oscillation in the length of the interferometers arms. The signal is obtained by the difference on the arm's length induced by the passage of a GW, which is visible as an interference pattern. Each detector is sensitive to a part of the sky, for example if a GW comes from the top of the detector, no signal will be detected. That's why it is interesting to have several detectors in different places on the Earth. Thereby the chance to detect a signal from every part of the sky will be higher.

1.2.2 Difficulty of detection

Actually, the noise makes the sensitivity of the interferometer! For instance, the first physical limit is given by the finite number of photons in the lasers which varies and then leads to a noise called the shot noise or the noise of photons. These fluctuations which are detected by the final photo-detectors reduce the contrast and the power of the laser which is the first "problem" to consider but not the last.

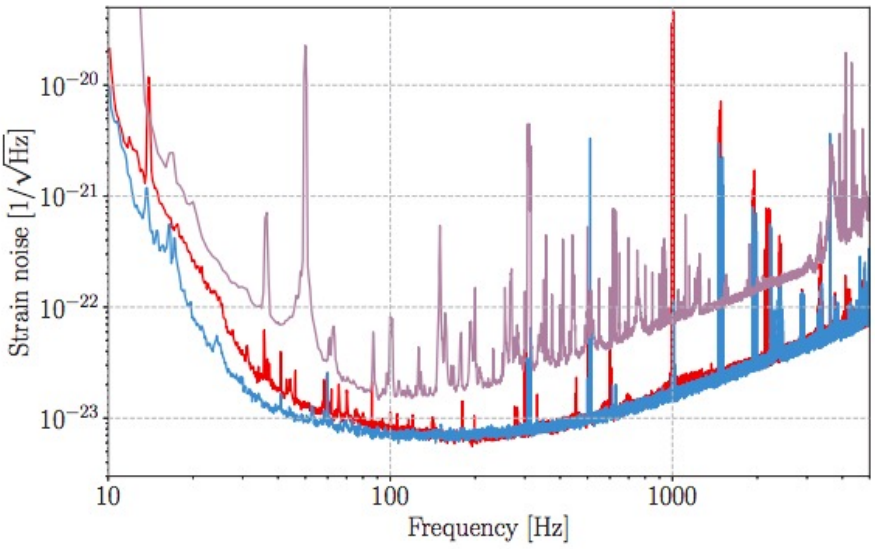

Figure 1.3: Amplitude spectral density of the total strain noise $h(t)$ which represents the amplitude of oscillations coming from noise of the Virgo,LHO and LLO detectors (the lower the curve is, the sensitivity the sensitivity) [1].

Because of the extreme smallness of the signal, a lot of external sources can parasite the data. Thereby,the main issue for these detectors is to avoid the noise from any intrinsic or environmental factor like thermal noises induced by the instruments themselves or seismic sources. Figure 1.3 shows the noise in each detector ,

as a a function of the frequency. The strain noise represents the amplitude of $h(t)$ oscillations coming from noise, so the lower the curve is, the higher the sensitivity.

The remaining noise is tackled directly at the analysis level with statistical tools and the theory of signal processing which we will discuss in the next part. Also, the detectors are placed in coincidence in order to decrease as much as possible the fakes signals coming from noise in any individual detector because the noises aren't correlated between detectors.

1.2.3 Present and futures detectors

The LIGO/Virgo instruments made the experimental GW science possible. During the latest observation run (called O3, that lasted since April 2019 until March 2020) LIGO and Virgo have observed an average of 1 interesting event per week. The interferometers are now undergoing a technical shutdown, with several foreseen improvements, which will lead to an even higher sensitivity for the next observation run (O4 in 2021).

Besides, new detectors are also operating in project, terrestrial such as:

- KAGRA in commissioning phase and already taking data.
- LIGO India same as LIGO but in India, the site has been chosen, but the construction has not started yet.

- 4^{th} generation of detectors such as Einstein Telescope in Europe or Cosmic Explorer in USA (still in the project phase and not approved yet).

And one space-based detector LISA which is an approved project and already funded. It will be composed of three satellites and will be sensitive to lower frequencies, Figure 1.4.

1.3 CBC searches

The Virgo group at IP2I works on offline detection of CBC with the MultiBand Template Analysis code [2]. It exists two kind of analysis: offline and online. The online analysis is performed live during data taking in order to alert the telescopes with the lowest possible latency. So that for interesting events (like the coalescence of two neutron stars) they can point to the correct sky localisation and provide an electromagnetic followup. The offline analysis is released several weeks after the data taking and allows to have a better estimation of parameters and a better sensitivity.

The purpose of the analysis is to detect signals of coalescence between two neutron stars -BNS-, or a neutron star and a black hole -BHNS-, or two black holes

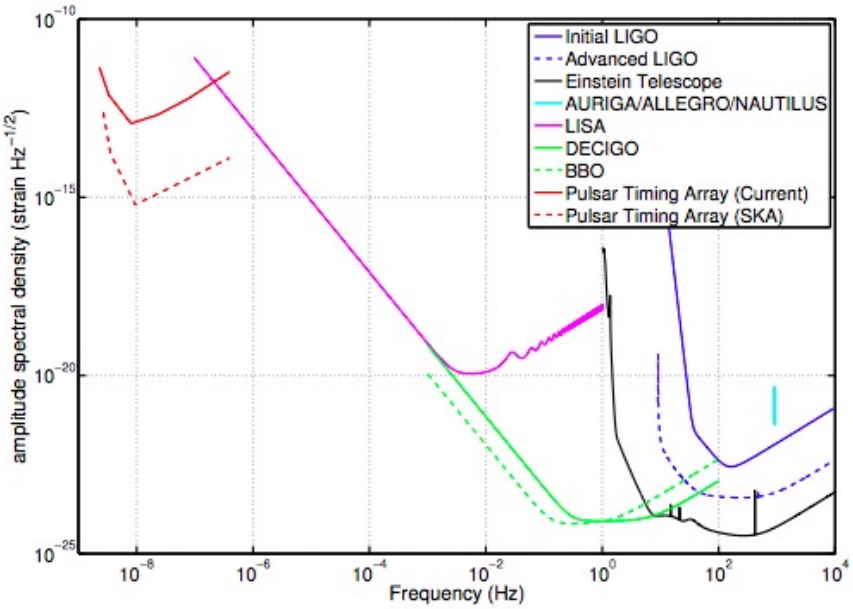

Figure 1.4: Improvements of the sensitivity of detectors as a function of the frequency

-BBH- on the data of LIGO and Virgo. CBC analysis use a matched filtering technique, that will be explained in the following. The basic idea is to evaluate the compatibility of the data with several theoretical waveforms (templates) and see if any of them has a good matching. From this procedure,we estimate the significance of an event by computing its Signal on Noise Ratio (SNR) and the chance that the event is just coming from the noise which is quantified by the False Alarm Rate (FAR). Let's see how these two variables are built.

-SNR:

We have to introduce the Fourier transform and the intercorrelation product to really understand the matched filtering.
The Fourier transform is defined as:

$$\tilde{a}(f) = \frac{1}{\sqrt{2\pi}} \int_{-\infty}^{+\infty} a(t) e^{-i2\pi f t} dt \tag{1.6}$$

Let's consider two different signals a_1 and a_2, the intercorrelation product is defined as :

$$a_1 \star a_2 = \int_{-\infty}^{+\infty} a_1(t) a_2(t+\tau) dt \tag{1.7}$$

This product quantifies how much two signals are corresponding as it is explained Figure 1.

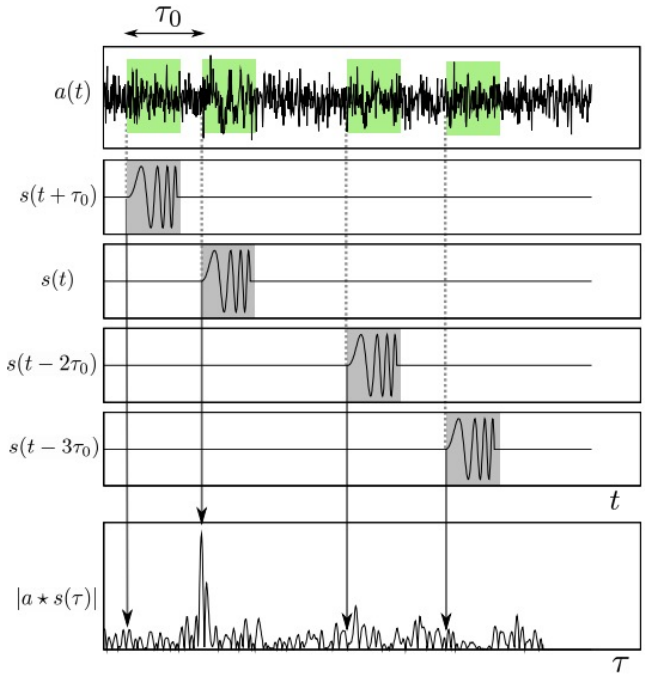

Figure 1.5: Explanation of the intercorrelation product between two signal $a(t)$ and $s(t)$ where $a(t)$ is built as the sum of the signal $s(t)$ at a time τ_0 and a random Gaussian noise

Then, we perform the product between the signal in the output of the detectors $h(t) = n(t) + s(t)$, with $n(t)$ the noise and $s(t)$ the signal, and a template:

$$S \equiv | \tilde{h} \star s(\tau) | \tag{1.8}$$

Next, we compute the standard deviation of a signal which contains only noise:

$$\sigma_N = \sqrt{\langle n \star s(\tau)^2 \rangle - \langle n \star s(\tau) \rangle^2} = \sqrt{\langle n \star s(\tau)^2 \rangle} \tag{1.9}$$

where $\langle\rangle$ is the average value over time. Besides $\langle n \star s(\tau) \rangle = 0$ because the noise $n(t)$ and the signal $s(t)$ are totally different.

And then we define the ratio of S and σ_N called Signal on Noise Ration -SNR- which assesses how strong the signal is relative to the noise :

$$SNR \equiv \frac{S}{\sigma_N} \tag{1.10}$$

Thus, the greater the value of the SNR is, the greater the chance that the signal comes from a real event will be.

-FAR:

The False Alarm Rate is the rate expected from background-only events. Without going into details, in MBTA, it is evaluated making all possible combination of

signals from the three detectors, hence building "fake" coincidences and measuring their rate. Several re-scaling factors are then needed to obtain a rate that is meaningful, based on the observation time and considered searches.

The FAR associated to an observation helps quantifying how likely it is that it comes from a real event and not a fluctuation of the noise. For instance we can see Figure 1.6, the grey band that shows the expected noise from background only and the red curve and the blue dots which are the observations. The blue dots that are significantly far from the background expectations corresponds to events that were judged significant enough to be tagged as real.

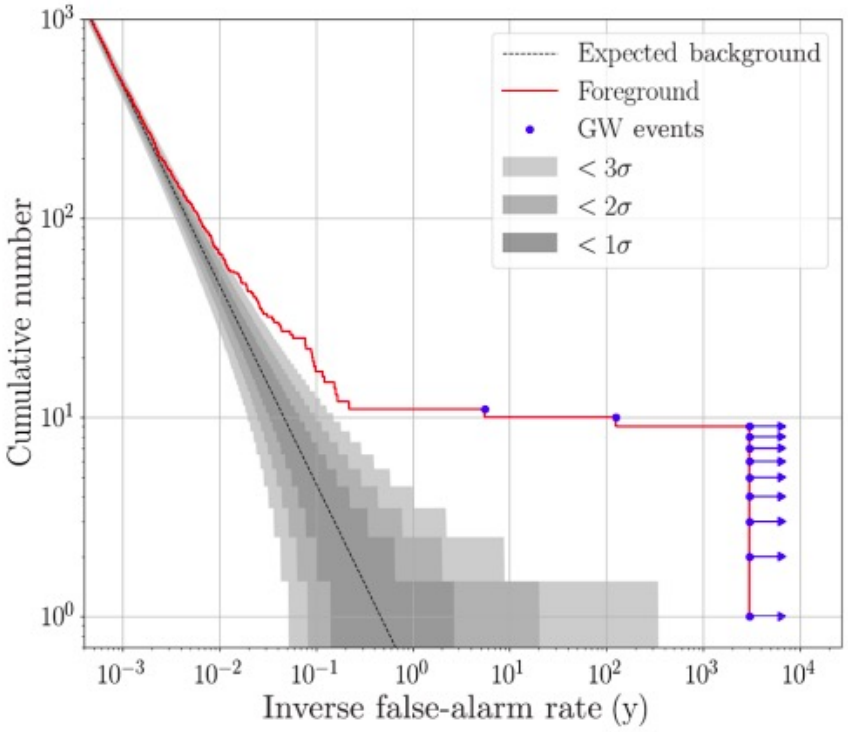

Figure 1.6: Cumulative histograms of search results for the matched-filter searches plotted verse inverse FAR. The Figure is taken form the LIGO/Virgo publications on the second observation run [2].

Before running on data to look for candidates, simulated events are superimposed on data and the analysis is run to establish its performances. These simulated events are called injections and their contribution to $h(t)$ are based on waveform we would expect from real astrophysical events.

The standard procedure within the LIGO/Virgo working group is to first review the performances on simulations (and on noise from data) before assessing that the performances of the pipeline are acceptable and then proceeding to look for real candidates in data. Since the background changes all the time, this assessment has to be done very often (typically once a week). For all these reasons, the run on

simulations plays a central role in the offline CBC analyses.

During my internship, I have participated to the MBTA offline running, in particular concerning the run on data with injections.

As explained, the run on injections is very important to evaluate the performances of the analysis. Running over all data with overimposed simulated event, and testing a larger number of templates can be very CPU and time consuming. Since the assessment of performances has to be repeated roughly every week on a new chunk of data, it is important to optimise the CPU usage of the run on injections. The first part of my internship concerns this topic, and is documented in Chapter 2. In chapter 3, the evaluation of the performances of the analysis are summarised, in particular for that concerns detection efficiency and analysis sensitivity.

Chapter 2

Computing time and resources optimisation for simulation runs

2.1 Introduction

2.1.1 Purpose

As we have seen before, the study consists on a matching between data and templates. The number of templates is very high (e.g. 170 000 for BBH) and we have to optimize the resources usage for the run on simulated events which, as explained, has to be performed roughly every week.
The basic idea is, for each injection, instead of performing the matched filtering for all templates, to use only the templates that are close (in the parameter space) to the simulated event.

So, for each injection , we choose a parameter of the injection such as the mass for instance and we match the templates which are in a certain interval in mass around the value of the corresponding injection. By doing that we have a gain in computation time but, at the same time, we can lose injections that would have been detected by templates with a mass value outside the considered interval. Thus,we have to find a good equilibrium between the gain in time and the relative lose of injections that we arbitrary want to smaller than 2%.

At first, a study has been performed to determine which variables are best suited to make the selection of templates to be used ,given an injection. The main variables

considered here are the following:

$$\chi = \left(1+\frac{(m_1-m_2)}{(m_1+m_2)}\right)\frac{S_{1Z}}{2m_1^2}+\left(1-\frac{(m_1-m2)}{(m_1+m_2)}\right)\frac{S_{2Z}}{2m_2^2}, \quad (2.1)$$

$$M_{chirp} = \frac{(m_1m_2)^{3/5}}{(m_1+m_2)^{1/5}}, \quad (2.2)$$

$$S_{TOT} = S_{1Z}+S_{2Z} \quad (2.3)$$

$$M_{TOT} = m_1+m_2 \quad (2.4)$$

$$\eta = \frac{m_1m_2}{(m_1+m_2)^2} \quad (2.5)$$

$$(2.6)$$

where $m_{i=1,2}$, are the masses of the two coalescing objects and $S_{i=1,2\ Z}$ the projections along the z axis of their spin.

2.1.2 Strategy

The strategy used to quantify the gain in time and the loss of information is the following:

1) The first step is to run using all templates , without any cut , with all the injections to have a concrete view of the matching between the templates and the injections and see the performances without cuts.

2) For each considered variable X, we build the quantity $\Delta = X_{det} - X_{inj}$, where X_{det} is the value of X for the template that has resulted in a detection and X_{inj} is the true value used to generate the injection.Δ is calculated for each detection corresponding to an injection and its dispersion measures how well we reconstruct the variable X.

3) From the study of Δ, one can determine:

i. the fraction of injections we would have missed if we had cut on X, as a function of the cut value. As stated previously, we define as our target that this fraction must not be higher than 2%.

ii. the corresponding fraction of used templates; this quantifies the gain in time when running on data with overimposed injections.

As we will see, the same procedure can be adapted to more complicated cases (variable cut, 2-dimensional cut using 2 variables,..).

4) In future runs, the selection can be used right away, resulting in an optimal usage of CPU time and resources.

5) The whole procedure is repeated for each kind of search (BBH,BNS and BHNS). Given the number of available templates (around 170 000 for BBH, 260 000 for BNS and 500 000 for BHNS), the reduction of computing time needs for BHNS will have the strongest impact on the analysis.

2.2 Results

2.2.1 BNS

This section describes the results of the procedure explained in 2.1.2, for binary systems of Neutron Stars.

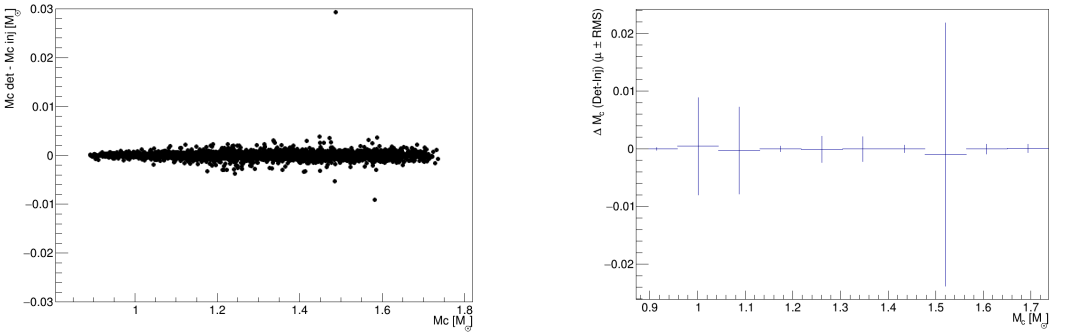

(a) ΔM_{chirp} as a function of M_{chirp}

(b) Profile of M_{chirp} as a function of M_{chirp}

Figure 2.1: Left plot: dispersion of M_{chirp}, on the x axis is displayed the value of M_{chirp} of the injection and on the y axis $\Delta = M^{Det}_{\text{chirp}} - M^{Inj}_{\text{chirp}}$. Each point corresponds to a detected injection. Right plot: for each bin in M_{chirp}, the points show the average value of Δ for detected injections with M_{chirp} falling in the considered bin.The error bars show the RMS of the Δ distribution.

The Figure 2.1(a) shows the dispersion in ΔM_{chirp} as a function of the value of the injected M_{chirp} and we can see that the resolution is very good because we have a small dispersion.

The Figure 2.1(b) shows to us the mean value of ΔM_{chirp} as a function of the injected M_{chirp} with RMS as errors for the bins. The differences in RMS between adjacent bins are driven by few outlier events, resulting from bad matching, some of which are not visible in (a).

As a first step, we use a constant cut of $\Delta M_{\text{chirp}} < 0.01 M_{\odot}$. The performance of such choice are displayed in fig 2.2.

Figure 2.2(a) represents the fraction of used templates. The red histogram shows, for the central value of each M_{chirp} bin, the fraction of templates that lie

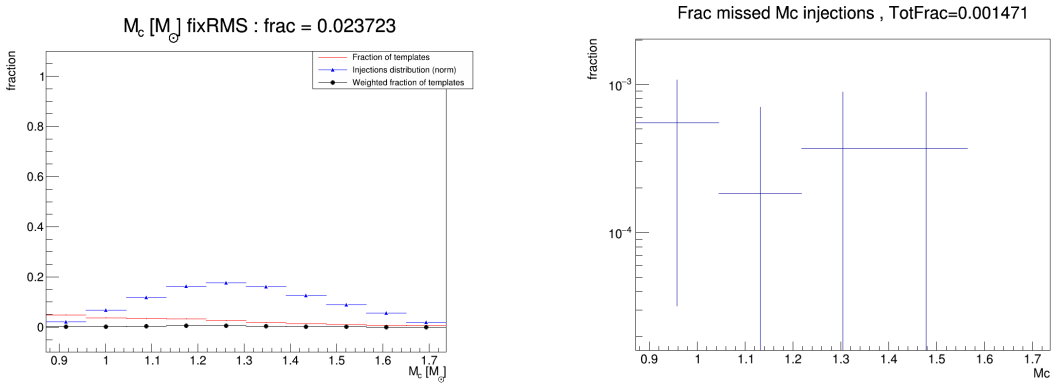

(a) fraction used templates

(b) fraction missed injections

Figure 2.2: Results of the 1D study -BNS-

within an interval of $\pm 0,01 M_{\odot}$, the blue one is the normalised distribution of injections and the black one is the multiplication of the red by the blue in the purpose to have a weighted average. Then, by integrating the black bins, we get the fraction of used templates which is here equal to $2,4\%$.

Figure 2.2(b), shows the fraction of missed injections. Each bin represents the number of missed injections in the bin divided by the total number of injections. The total fraction of missed injections is to 0.1%.

In conclusion for the BNS system, if when running on injections we use a constant cut of $\pm 0,01 M_{\odot}$, to determine which templates to use, we expect to improve by a factor 50 the running time related to the matched filtering step. This reduction comes with a loss of injections of about 1 per thousand. The performances of the method being very satisfactory already in this simple scenario (constant cut), we don't try more complicated solutions.

2.2.2 BHNS

The second system -Black Hole Neutron Star- is very important because of its number of templates (around 500 000). Then that's where we want to absolutely have the bigger gain as possible, in our computation time.
We have remade the previous study to find out the best variable of interest for such system. It appeared that M_{chirp} is again the best variable with the lowest dispersion. In Figure 2.3 (a) and (b), the dispersion in ΔM_{chirp} seems to depend on the value of the considered injected M_{chirp}.

In this case we consider a variable cut, meaning that the value used to choose which templates to consider will change from one injection to another. Several values of the cut are tested, as shown in Figure 2.4 and Table 2.1.

From this study, and keeping in mind we want to have less than 2% of missed

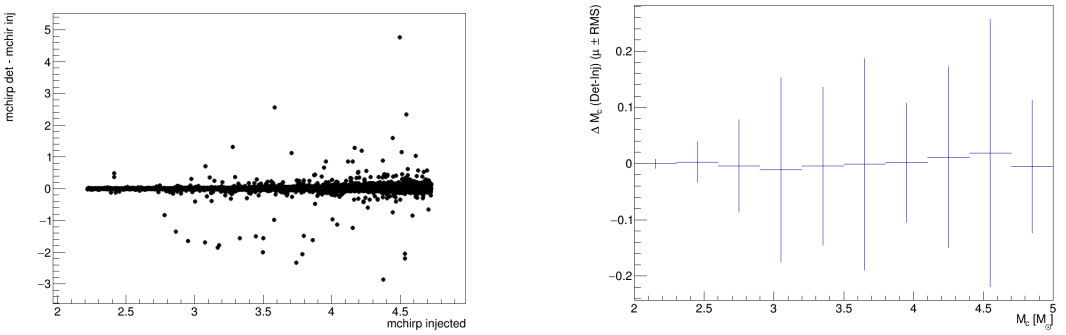

(a) ΔM_{chirp} as a function of M_{chirp}

(b) Profile of M_{chirp} as a function of M_{chirp}

Figure 2.3: Left plot: dispersion of M_{chirp}, on the x axis is displayed the value of M_{chirp} of the injection and on the y axis $\Delta = M^{Det}_{\text{chirp}} - M^{Inj}_{\text{chirp}}$. Each point corresponds to a detected injection. Right plot: for each bin in M_{chirp}, the points show the average value of Δ for detected injections with M_{chirp} falling in the considered bin.The error bars show the RMS of the Δ distribution.

injections, the best solution for BHNS is to use a cut on M_{chirp} corresponding to $2 \cdot RMS$, see Figure 2.4 and Table 2.1. This means that, when running on a given injection simulated with a value of M_{chirp}, we only considered the templates whose M_{chirp} is within $\pm 2 \cdot RMS$ of the injected value. The used RMS is the error bar shown in fig 2.3(b) for the bin corresponding to the considered value of M_{chirp}.

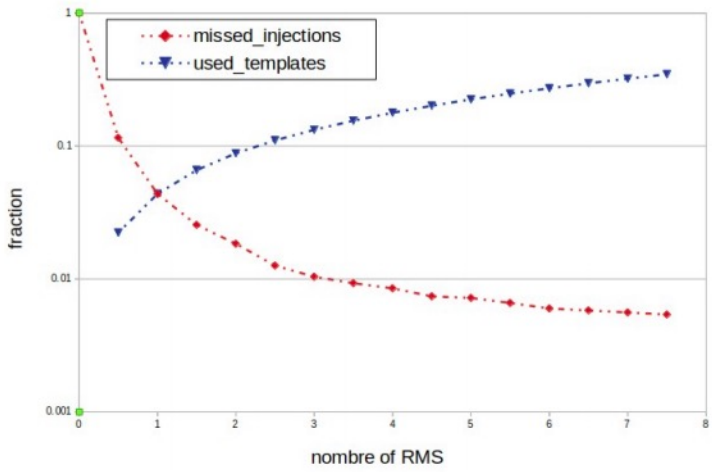

Figure 2.4: Graphs of fractions as a function of n

With this cut , we use 9% of all templates for a loss of $1.8\% \pm 0.2\%$ of all the injections, as visible in Figure 2.5.

To conclude for the BHNS case, we have found that a variable cut on M_{chirp}, equal to $2 \cdot RMS$, will give us a factor ~ 10 gain in computing time and a corresponding loss of injections of 1.8%.

Number of RMS	Fraction used templates (%)	Fraction missed injection (%)
0.5	2.2	11
1.0	4.4	4.4
1.5	7	2.5
2	9	1.8
2.5	11	1.3
3.0	13	1.0

Table 2.1: Summary of BHNS results for different n

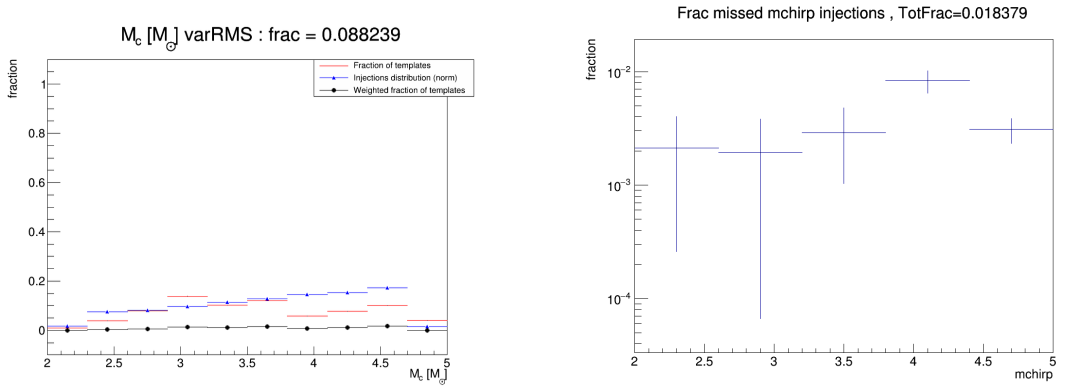

(a) fraction used templates

(b) fraction missed injections

Figure 2.5: Results of the 1D study -BHNS-

2.2.3 BHH

The last system -BBH- is the more complicated because at high masses the analysis has its worst reconstruction resolution of physical quantities, due to shorter signals, more difficult to characterize. This will be visible as a larger dispersion in our plots. Again , as previously ,M_{chirp} seems to be the best variable for beginning the study.

Figure 2.6 shows the dispersion of M_{chirp} indicating that we have to consider a variable cut to obtain the best gain as possible.

The performances of different value of the variable cut are summarized in Fig 2.7 and Table 2.2. The best solution appears to be a cut at $7 \cdot RMS$ which gives us a fraction of used templates equals to 28% for a corresponding loss of injections of $2.0 \pm 0.3\%$.

A time gain factor of 3 not being enough, we have decided to continue the study with two variables: M_{chirp} and χ. We consider the same Figures of merit as previously (the fraction of used templates and the fraction of missed injections), but this time we evaluate them in the case where we select the templates based on two

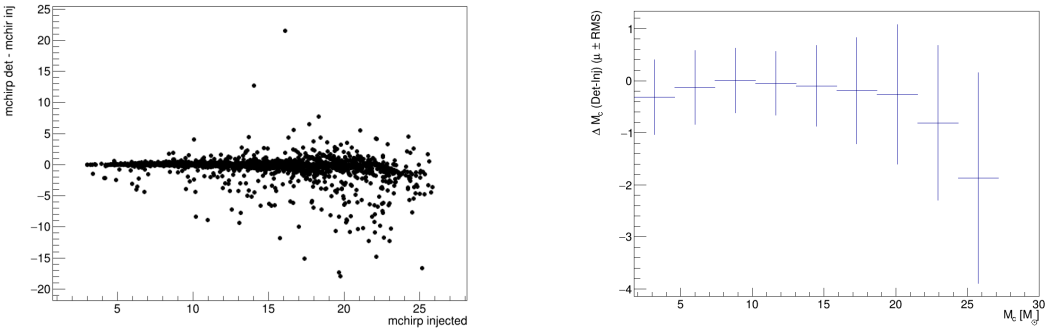

(a) ΔM_{chirp} as a function of M_{chirp}

(b) Profile of M_{chirp} as a function of M_{chirp}

Figure 2.6: Left plot: dispersion of M_{chirp}, on the x axis is displayed the value of M_{chirp} of the injection and on the y axis $\Delta = M^{Det}_{\text{chirp}} - M^{Inj}_{\text{chirp}}$. Each point corresponds to a detected injection. Right plot: for each bin in M_{chirp}, the points show the average value of Δ for detected injections with M_{chirp} falling in the considered bin.The error bars show the RMS of the Δ distribution.

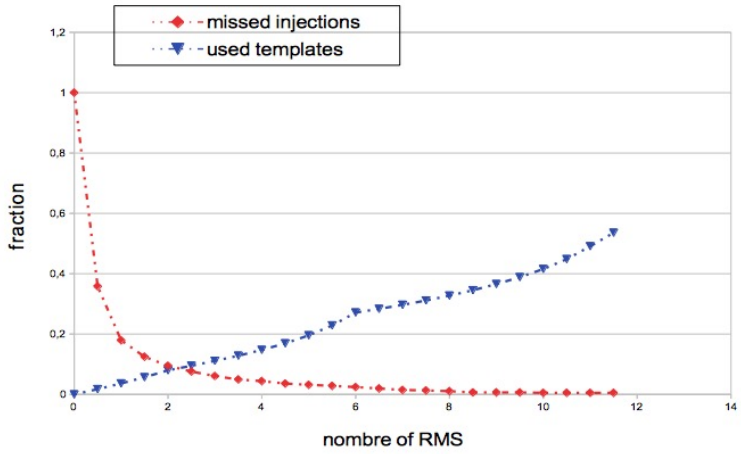

Figure 2.7: Graphs of fractions as a function of n

Number of RMS	Fraction used templates (%)	Fraction missed injection (%)
2	8	10
3	11	6.1
4	15	4.3
5	20	3.2
6	27	2.4
7	30	1.5
8	33	1.1

Table 2.2: Summary of BBH results for different n

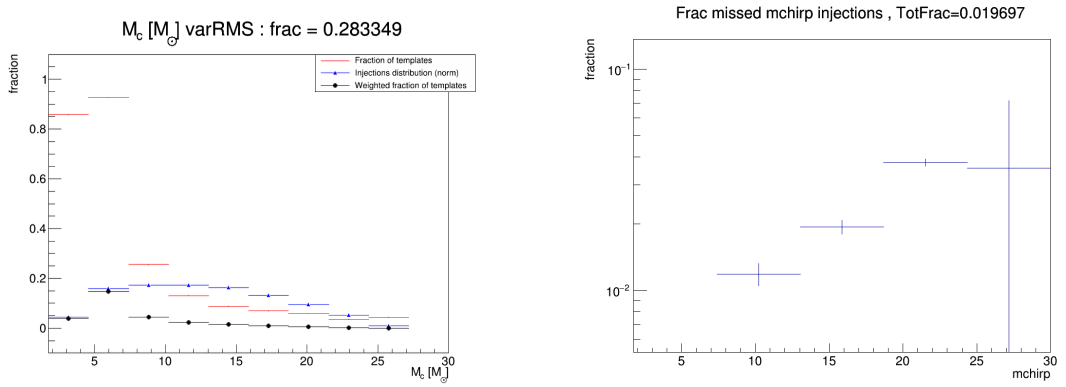

(a) Fraction used templates (b) fraction missed injections

Figure 2.8: Results of the 1D study -BBH-

variables. In other words, for an injections with a given value of M_{chirp} and χ, we only consider templates that have these two variables in two given interval.

An extension of the described method to the case of 2 variables allowed us to determine the best selection to apply, which seems to be to consider templates that have values of M_{chirp} and χ within respectively $7 \cdot RMS_{M_{\text{chirp}}}$ and $2.5 \cdot RMS_{\chi}$.

With this selection, we get a fraction of used templates equals to 21% for a corresponding loss of injections equals to $1.8 \pm 0.3\%$ as we can see in the Figure 2.9. The two graphs shown are the equivalent of the previous graphs but two dimensional. Indeed, the plot (a) Figure 2.9 is the equivalent of the black histogram shown, for example in Figure 2.8(a), while by integrating the bins of graph (b) of Figure 2.9 we get the fractions of missed injections.

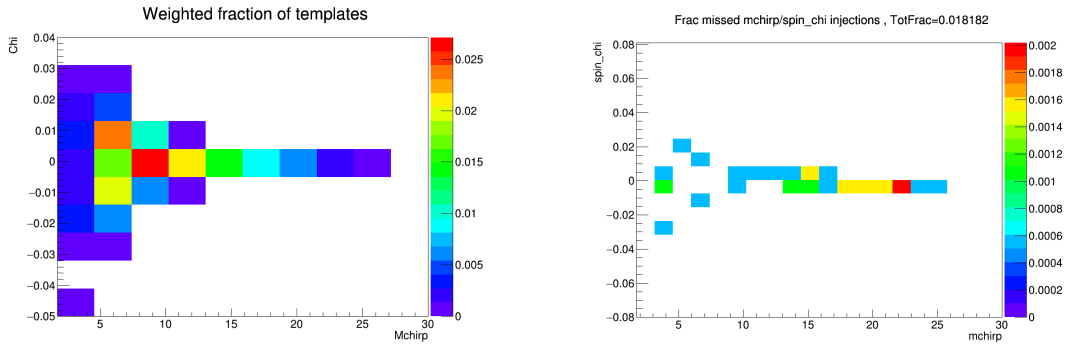

(a) Fraction used templates (b) fraction missed injections

Figure 2.9: Results of the 2D study for BBH: the left plot shows in y and x axis the values of Δ for M_{chirp} and χ and the color corresponds to the fraction of used templates in the bin. The color code in the right plot shows, for each bin, the fraction of missed injection.

In summary for BBH, the best solution seems to be a variable cut with M_{chirp} and χ resulting in a factor 5 gain computational time and a loss of 1.8% of all the

injections. BBH is the system with the lowest gains which is no surprising because of the difficulty explained at the beginning.

2.3 Conclusion

The optimal cuts, with their performances, are summarized in the Table 2.3.

System	Cut	Cut value	Gain in time	Injections loss (%)
BNS	fixe	$0.01 M_{\odot}$	50	0.1
BHNS	variable	$2 \cdot RMS$	11	1.8
BBH	variable	$7 \cdot RMS_{M_{\text{chirp}}} - 2.5 \cdot RMS_{\chi}$	5	1.8

Table 2.3: Summary of results for different systems

The results presented previously were obtained using the data from the first week of 2019 LIGO/Virgo running, called chunk1. As shown in Figure 2.10, the performances have been tested on three other similar periods (chunk4, 5 and 6) and appear to be very stable.

A selection of templates, according to the values determined with this study, is now used by the nominal analysis. In the future, this study can be repeated with some improvements such as including more stringent selection on the SNR or FAR of the considered events, in order to minimise the impact of fakes detections.

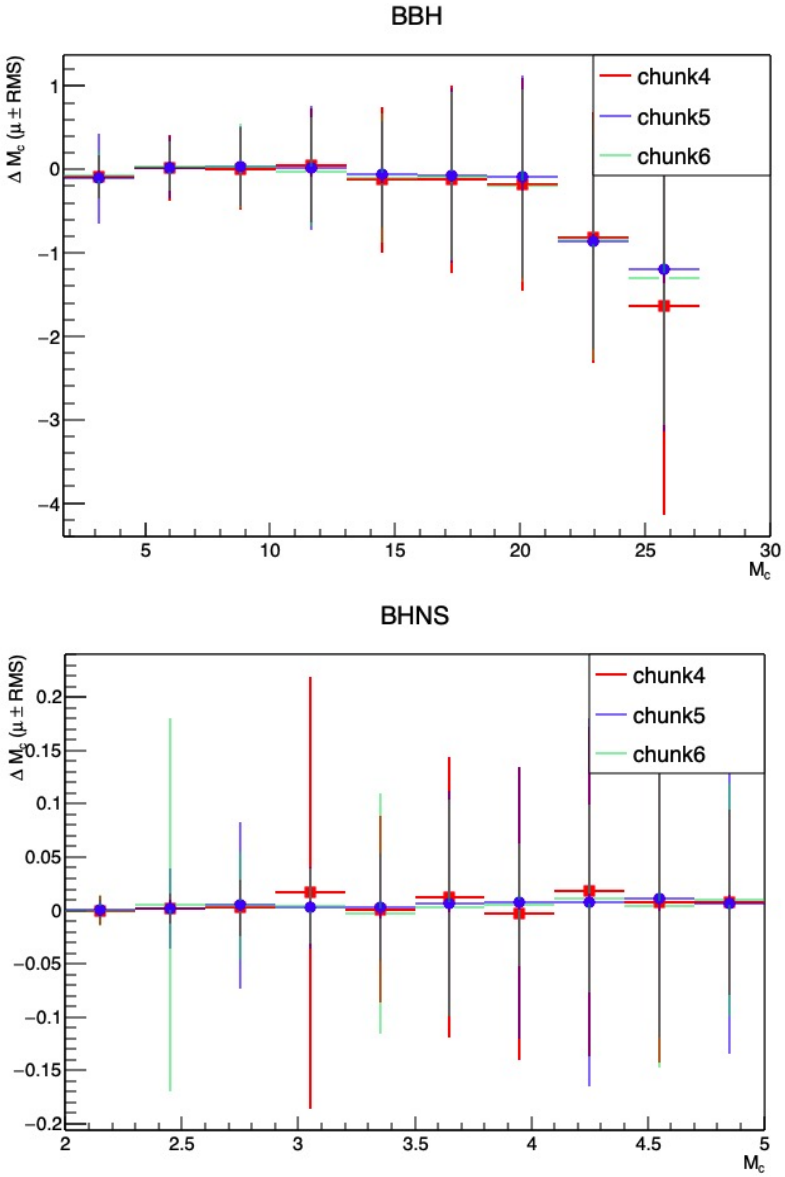

Figure 2.10: Delta M_{chirp} as a function of M_{chirp} for different chunks

Chapter 3

Determination of the sensitivity of the analysis

3.1 Description

This section documents the evaluation of the sensitivity of the MBTA offline analysis. In particular, we are interested to see the efficiency of the analysis, as a a function of some interesting variables. The efficiency is defined as the number of detected events (with a signal on noise ratio of at least 5).

3.2 Results

For technical reasons the injections are generated homogeneously in distance, while in real model, we can expect them to be distributed uniformly in volume instead. In order ti recover the correct distributions a weight s applied to the generated events.

The maximum distance for the considered injections campaign is 5000 Mpc for BBH, 750 Mpc for BHNS and 350 Mpc for BNS. We can see Figure 3.1, that the efficiency of recovering BBH events does not plateau at 100% even for close distances. The reason is that for high masses the GW waves signals are very short, and are tagged as noise "glitches" by the MBTA code. To recover such signals, a parallel search is run, with no protection against glitched, and only considering very short templates. These additional detected events are not included in the plot shown in Fig 3.1.

Figure 3.2, shows the efficiency as a a function of the effective distance of the Livingstone detector (LIGO). The effective distance is the actual distance of the source multiplied by some geometrical factors, and represents the distance at which the source localised in the maximum sensitivity spot for a given detector, would give a signal of the observed amplitude.

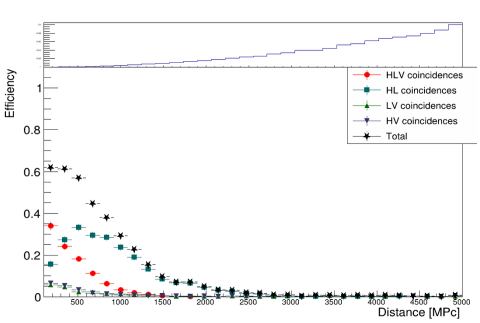

(a) *BBH*

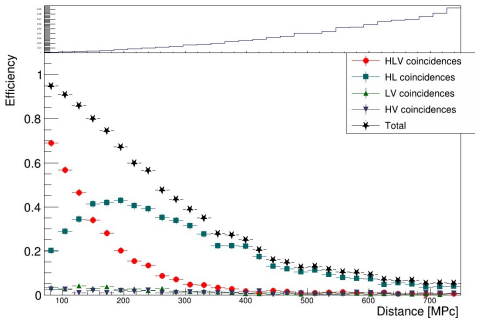

(b) *BHNS*

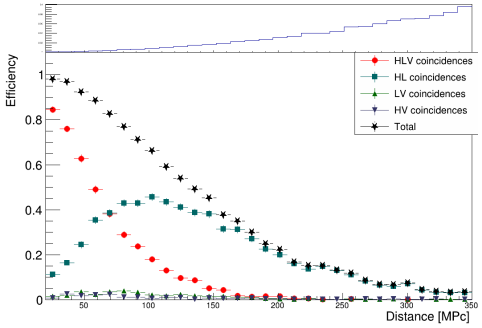

(c) *BNS*

Figure 3.1: Efficiency as a function of distance[Mpc]

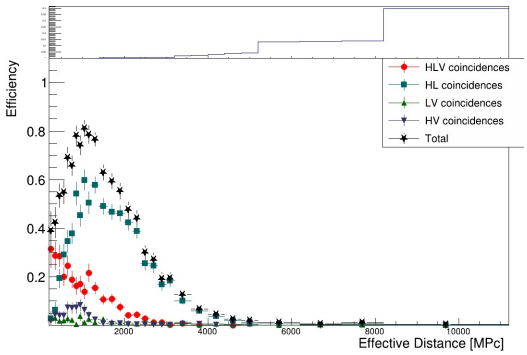

Figure 3.2: Efficiency as a function of the effective distance -BBH-

Finally, Figure 3.3 shows the sensitive distance, defined as the distance that we can detect an event with a signal on noise ratio of at least 5, as a a function of the cut on SNR and on the IFAR which is the inverse of the FAR. As we can see, the higher the cut on SNR and IFAR is, the lower will be the sensitive distance. We can also notice that BBH seems to have a better sensitive distance than BNS and BHNS. This is explained by the fact that black holes have higher masses than neutron stars and a bigger mass will lead to a bigger signal amplitude. So, we can detect BBH system farther than BNS or BHNS system which explain this difference.

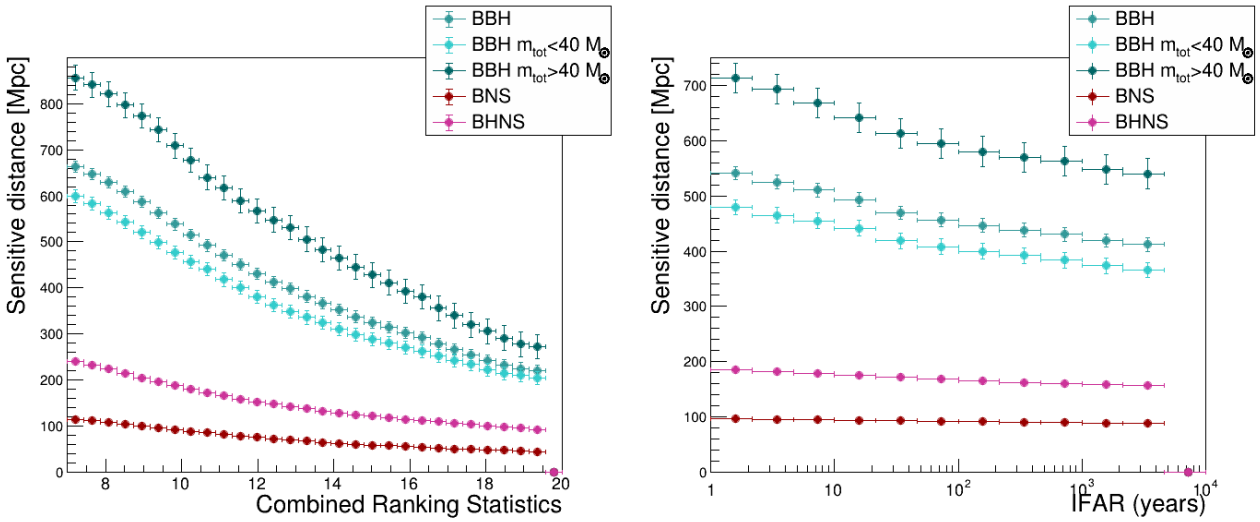

Figure 3.3: Sensitive distance as a function of the cut on SNR and IFAR for BBH

Chapter 4

Summary

My internship concerned the search for GW signals from CBC with the MBTA code. In particular, I have worked on the runs on simulated events (called injections and superimposed to real data).

First, I have developed a technique to optimise the usage of CPU and computing time for such runs, that allows the analysis to be 5-50 times faster.

As a second topic, I have analysed the results of the runs on simulated event and evaluated the efficiency and sensitivity of the analysis. With the current analysis setup, we are sensitive to coalescence of neutron stars up to a distance of around 100 Mpc, and up to almost 1 Gpc for coalescences of black-holes of about 40 solar masses.

Bibliography

[1] LIGO and Virgo scientific collaboration. *Properties of the Binary Neutron Star Merger GW170817,Phys. Rev. PHYSICAL REVIEW X9, 011001 (2019)*.

[2] LIGO and Virgo scientific collaboration. *GWTC-1: A Gravitational-Wave Transient Catalog of Compact Binary Mergers Observed by LIGO and Virgo during the First and Second Observing Runs,Phys. Rev. X9, 031040 (2019)*.

[3] T. ADAMS. *Low latency search for compact binary coalescences using MBYA,arXiv:1507.01787*.

Damir Buskulic. *Ondes gravitationnelles: aspects théoriques et expérimentaux*.

Kipp Cannon, Chad Hanna and Drew Keppel *A method to estimate the significance of coincident gravitational-wave observations from compact binary coalescence,arXiv:1209.0718v1*

Kipp Cannon, Chad Hanna and Jacob Peoples *Likelihood-Ratio Ranking Statistic for Compact Binary Coalescence Candidates with Rate Estimation,arXiv:1504.04632v1*

Dal Canton, Tito *Efficient searches for spinning compact binaries with advanced gravitational-wave observatoriesarXiv:gr-qc/0604037*

Acknowledgements

I would like to thank a lot Viola Sordini and Roberto Chierici for trusting me in this internship. In particular, Viola for her kindness and patience and her invaluable help in drafting this report.